Advanced Journal of Chemistry, Section A

Journal homepage: www.ajchem-a.com

Original Research Article

Exploring Quinazolinone Compound as Corrosion Inhibitor for Mild Steel in Acidic Media: Electrochemical and Theoretical Studies

Hind Malki[1], Otmane Kharbouch[1], Fatima Hamouche[1,2,*], Nadia Dkhireche[1], Khalil El Mabrouk[2], Fatima Elhajri[3], Zakaria Benzekri[3,4], Said Boukhris[3]

[1]*Advanced Materials and Process Engineering, Faculty of Sciences, Ibn Tofaïl University, PO Box 133, 14000, Kenitra, Morocco*
[2]*Euromed University of Fez, Fez, Morocco*
[3]*Laboratory of Organic Chemistry, Catalysis and Environment, Department of Chemistry, Faculty of Sciences, Ibn Tofail University PO Box 133, 14000, Kenitra, Morocco*
[4]*Laboratory of Heterocyclic Organic Chemistry, Mohammed V University in Rabat, Faculty of Sciences Av. Ibn Battouta, BP 1014 Rabat, Morocco*

ARTICLEINFO

Article history

Submitted: 2025-12-07
Revised: 2025-12-20
Accepted: 2026-01-28
ID: AJCA-2512-1994
DOI: 10.48309/AJCA.2026.546165.1994

KEYWORDS

Sustainable development
Mild steel
Quinazolinone derivative
Inhibitor
Atom-in-molecule theory

ABSTRACT

This study examines the corrosion inhibition efficacy of a novel quinazolinone derivative, 1'*H*-spiro[cyclohexane-1,2-quinazolin]-4'(3'*H*)-one (ZB5). The compound was characterized by ^{13}C-NMR and ^{1}H-NMR spectroscopy, and its corrosion inhibition activity on mild steel was evaluated in a 1.0 M HCl solution using potentiodynamic polarization (PDP) and electrochemical impedance spectroscopy (EIS). ZB5 demonstrated remarkable protection, with an inhibition efficiency of 82.83% at 10^{-3} M. Adsorption studies revealed that ZB5 follows the Langmuir isotherm model, confirming monolayer adsorption on the MS surface. Surface characterization by SEM/EDS, XRD, and FTIR confirmed the formation of a protective layer, while ICP-OES analysis provided information on elemental composition and ion release. Further density functional theory (DFT) calculations and Monte Carlo (MC) simulations established a strong correlation between the electronic structure of ZB5 and its adsorption behavior, thus confirming the experimental results. Overall, this work provides robust experimental and theoretical evidence for ZB5's strong corrosion-inhibiting capacity, highlighting its potential as an effective protective agent for mild steel in acidic environments.

* Corresponding author: Hamouche, Fatima
✉ E-mail: Fatima.hamouche@uit.ac.ma

GRAPHICAL ABSTRACT

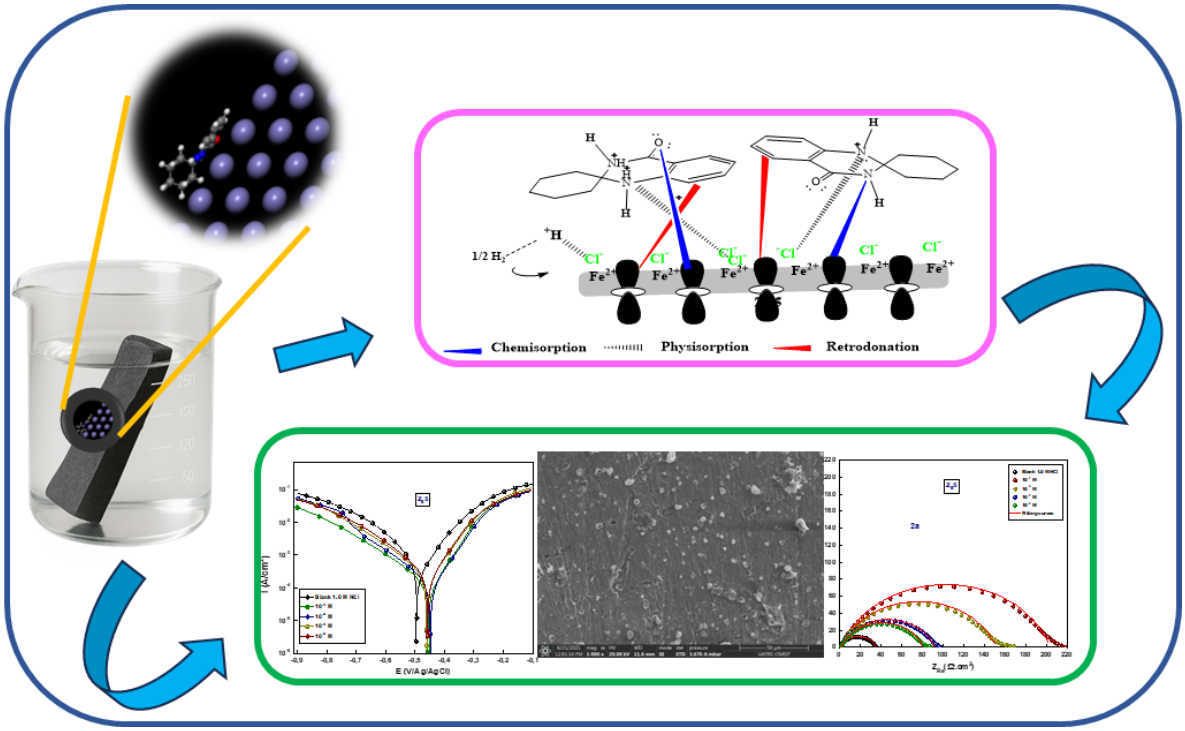

Introduction

Mild steel is widely used in various technical applications, including storage tanks, heat exchangers, pipelines, acid manufacturing, power generation, and the oil industry [1]. However, it has a significant limitation regarding corrosion resistance, particularly in acidic environments where exposure to hydrochloric acid (HCl) poses a considerable challenge [2]. Corrosion, the degradation of metallic materials due to chemical or electrochemical reactions with their environment, can lead to deterioration of the metal's properties. This degradation often results in substantial economic losses across industrial sectors, including equipment failures, increased maintenance costs, and diminished operational efficiency [3,4]. Therefore, addressing corrosion in mild steel is crucial for extending equipment lifespan and minimizing associated expenses.

One practical approach to mitigate corrosion is the use of organic inhibitors, chemical compounds designed to slow or prevent corrosion by forming a protective layer on the metal surface [5]. These inhibitors primarily function through adsorption, effectively creating a barrier that blocks corrosive agents [6]. Their effectiveness, relatively low costs, and ease of applications in various corrosive environments, including acidic media, make them highly valued in industrial settings [7]. The adsorption of these organic inhibitors is significantly influenced by their physicochemical properties, such as functional groups, the electron density of donor atoms, and potential steric effects [8,9]. These factors play a vital role in determining the inhibition potential, primarily through substitution effects.

Over the years, numerous organic compounds have proven to be effective corrosion inhibitors, including imidazoles [10], quinolines [11], and quinazolines [12]. These compounds have shown a high efficacy in various corrosive environments by forming protective films on metal surfaces via adsorption, thereby significantly reducing

corrosion rates, especially in acidic media such as hydrochloric acid (HCl) [13]. Studies report a corrosion efficiency of imidazole-based inhibitors of up to 98% in a 5.0M HCl solution [14], an efficiency of 90% for quinoline derivatives [15], and an efficiency of 93% for a compound, 2-(3-pyridyl)-3,4-dihydro-4-quinazolinone, as a corrosion inhibitor for mild steel in a 0.1 M HCl solution [16]. Further research on three quinazoline derivatives as environmentally friendly corrosion inhibitors for carbon steel in 2 M HCl yielded an inhibition efficiency of 78%. Taken collectively, these findings highlight the potential of organic compounds as practical tools for combating corrosion in various acidic environments [17].

This study focuses on evaluating the corrosion-resistant properties of the quinazolinone derivative, 1'*H*-spiro[cyclohexane-1,2-quinazolin]-4'(3'*H*)-one, when applied to mild steel in a 1.0 M HCl acidic environment. The compound was synthesized and characterized using proton (^{1}H) and carbon (^{13}C) nuclear magnetic resonance (NMR) spectroscopy [18]. To evaluate the inhibitory performance of the organic compound, a combination of electrochemical techniques was applied. The surface morphology of mild steel was examined using scanning electron microscopy (SEM) coupled with energy-dispersive spectroscopy (EDS), while structural and chemical changes were further characterized by X-ray diffraction (XRD) and Fourier-transform infrared spectroscopy (FTIR). Solution analyses, conducted with and without the inhibitor, were performed using inductively coupled plasma optical emission spectroscopy (ICP-OES) to determine elemental composition and ion release. In parallel, Monte Carlo (MC) simulations and density functional theory (DFT) calculations were performed to correlate the molecular structure of the quinazolinone derivative with its corrosion-inhibition efficiency. This integrated experimental–computational approach offers valuable insights into the relationship between molecular properties and corrosion resistance.

Experimental

Synthesis of organic compound ZB5

Aromatic aldehydes (4-chlorobenzaldehyde and 2,4-dichlorobenzaldehyde) (1 mmol), 2-aminobenzamide 2 (1 mmol), and $(N_2H_5)2SiF_6$ (0.1 mol%) were mixed in 2 mL of ethanol and heated to 80 °C with continuous stirring. The reaction progress was monitored by TLC using a solvent system of ethyl acetate and petroleum ether (1:4, v/v). Once the reaction was complete, hot ethanol was added to the mixture. $(N_2H_5)2SiF_6$ was recovered by essential filtration and, after cooling, the product was recrystallized from ethanol [18].

The working electrode and test solution

The mild steel used in this study for all corrosion experiments had the following composition (by weight): 0.09% P, 0.38% Si, 0.01% Al, 0.05% Mn, 0.21% C, and 0.05% S, with Fe as the balance. Small cylindrical mild steel bars were embedded in a plastic rod so that only the planar bottom surface (area 1 cm^2) was exposed to the test solution. Before each electrochemical measurement, the working electrode was polished with abrasive paper of varying grit sizes, rinsed with distilled water, degreased with acetone, air-dried, and immediately immersed in the test solution. The quinazolinone derivative was prepared in concentrations ranging from 10^{-6} M to 10^{-3} M, with a blank solution prepared for comparison. The aggressive HCl solution (1.0 mol/L) was obtained by diluting concentrated hydrochloric acid (37%) with distilled water.

Electrochemical measurements

A conventional three-electrode cell comprising a mild steel working electrode, spiral platinum wire

counter electrode, and Ag/AgCl (KCl sat.) reference electrode was used for the electrochemical measurements. A Gamry potentiostat surface 1010E was used for all experimental measurements. Gamry software was used to record data. The instantaneous potentiodynamic polarization (PDP) measurements were conducted in the anodic direction at a scan rate of 1 mV·s^{-1} from −900 mV to +100 mV relative to the open-circuit potential (OCP). The EIS measurements were performed at open-circuit potential (OCP) over a frequency range from 100 kHz to 100 mHz, with 10 points per decade. The amplitude of the applied AC signal was 10 mV/ms. All experiments were performed after 30 mn of mild steel immersion in 1.0 M HCl solutions in the absence and presence of different concentrations of the two studied compounds.

Surface analysis

Several advanced analytical techniques were employed to investigate the morphology, surface condition, roughness, and the nature of corrosion products formed on mild steel in hydrochloric acid. Surface characterization was performed using SEM coupled with energy-dispersive X-ray spectroscopy (SEM-EDS) with a FEI QUANTA FEG 450 instrument. Structural analysis was conducted by XRD with Siemens D5000 and Bruker AXS D8 instruments, while chemical bonding and functional groups were examined through FTIR using a BRUKER TENSOR II system. Data were collected both before and after exposure to the corrosive medium, in the absence or presence of the inhibitor, at room temperature.

Solution analysis

The elemental composition and ion concentrations produced on mild-steel surfaces in the presence of a corrosion-inhibiting molecule were explored using Inductively Coupled Plasma (ICP) spectrometry. Mild steel samples were immersed in a solution of 1.0 M HCl alone (blank) and a solution containing ZB5 for 48 h at 298 K.

Theoretical Framework

To understand how the quinazolinone derivative affects corrosion inhibition, a theoretical analysis was conducted using DFT. According to molecular orbital theory, examining the electron densities in the Highest Occupied Molecular Orbital (HOMO) and the Lowest Unoccupied Molecular Orbital (LUMO) can reveal the electrophilic or nucleophilic nature of different centers within a molecule. Specifically, HOMO is associated with a molecule's ability to donate electrons, while LUMO is associated with its ability to accept electrons [19,20]. Additionally, the Fukui functions were calculated to determine the nucleophilic or electrophilic nature of each atom in the quinazolinone derivative. These functions provide valuable insights into how different atoms within the molecule interact with reactive species. By analyzing the Fukui functions, it can better found which parts of the quinazolinone derivative are more likely to participate in electron-donating or electron-accepting processes, thereby influencing its effectiveness as a corrosion inhibitor [21–23].

DFT calculations

Using DFT optimization in Materials Studio 2017 (by Accelrys Inc.) [1], several quantum parameters were defined and examined to understand the relationship between chemical structure and inhibitory effectiveness. Among these parameters are the energies of the frontier molecular orbitals (ELUMO and EHOMO), which determine a compound’s ability to accept or donate electrons, thereby influencing its interactions with other molecules or chemical species [2,3]. The energy gap between bands (ΔE) serves as an indicator of a compound's stability and reactivity. A larger gap reflects greater stability and lower reactivity, whereas a smaller

gap may indicate higher reactivity [4,5]. Additionally, electronegativity (χ) measures an atom's ability to attract electrons in a chemical bond, playing a key role in bond polarity and intermolecular interactions [6]. Hardness (η) and softness (σ) are complementary concepts that respectively describe a compound's resistance to electronic changes and its propensity to undergo such changes [7]. Finally, the electron transfer fraction (ΔN) reflects changes in the electron distribution during a chemical reaction and significantly influences the properties and inhibitory effectiveness of the studied compounds [8]. The values of EHOMO and ELUMO are used to calculate these parameters using the following equations [9,10]:

$$\Delta E = E_{LUMO} - E_{HOMO} \quad (1)$$

$$\eta = \frac{E_{LUMO} - E_{HOMO}}{2} \quad (2)$$

$$\sigma = \frac{1}{\eta} \quad (3)$$

$$\chi = \frac{-(E_{LUMO} + E_{HOMO})}{2} \quad (4)$$

$$\omega = \frac{\chi^2}{2\eta} \quad (5)$$

$$\Delta N = \frac{\varphi - \chi_{inh}}{2(\eta_{Fe} + \eta_{inh})} \quad (6)$$

Where, ΦFe = 4.82 eV, and the value of the global hardness ηFe of iron is considered zero.

As a part of this study, the calculation of double Fukui descriptors, or second-order Fukui functions f_k^2, along with dual local softness $\Delta\sigma_k$ and dual local publicity $\Delta\omega_k$, was performed to identify the most reactive sites of molecules in their neutral or protonated states [11]. These descriptors, designed as analytical tools, enable in-depth exploration of local chemical reactivity. They highlight molecular regions, where significant interactions are likely to occur. The mathematical expressions defining these descriptors are as follows [12]:

$$f_k^2 = f_k^+ - f_k^- \quad (7)$$

Where, f_k^+ and f_k^- represent the Fukui indices of site k in cationic and anionic systems, respectively.

$$\Delta\sigma_k = \sigma_k^+ - \sigma_k^- \quad (8)$$

In this context, $\sigma_k^+ \; and \; \sigma_k^-$ designate the local softness quantities that describe nucleophilic and electrophilic attacks, respectively.

$$\Delta\omega_k = \omega_k^+ - \omega_k^- \quad (9)$$

Where, $\omega_k^+ - \omega_k^-$ correspond to local philic quantities describing nucleophilic and electrophilic attacks, respectively.

MC simulation

The molecular dynamics (MD) simulation method is used to develop a two-layer adsorption model using Materials Studio 2017. The first layer represents the metallic surface with the Fe (110) plane, and its dimensions are 37.24 × 37.24 × 14.19 Å^3 [13]. The second layer corresponds to the solvent layer and consists of 1 inhibitor molecule, 600 water molecules, 6 H_3O^+ ions, and 6 Cl^- ions. The solution and water layers are constructed using the Amorphous Cell module [14,15]. The COMPASSΠ force field is used to optimize the system, and the MD simulation is conducted in the canonical ensemble (NVT) using the Discover module. The MD calculations are carried out at 298 K, with an Andersen thermostat. The simulation time step is 1 fs, and the total simulation duration is 1,000 ps [16].

Results and Discussion

Potentiodynamic measurements

Figure 1 shows the I-E curves for mild steel in 1.0 M HCl at 298 K, both in the absence and presence of ZB5 at concentrations ranging from 10^{-3} M to 10^{-6} M. The electrochemical parameters, including the corrosion potential (E_{corr}), cathodic (β_c), and anodic (β_a) Tafel slopes, as well as the

inhibition efficiency (ηPP), are summarized in Table 1.

The results reveal exponential and parallel polarization curves, demonstrating that both the anodic iron oxidation and the cathodic hydrogen evolution are controlled by a charge-transfer mechanism, regardless of the presence or absence of the inhibitor [24]. These findings indicate that the inhibitor does not modify the fundamental reaction mechanisms of mild steel. The polarization curves display well-defined anodic and cathodic branches, confirming that corrosion proceeds through a pure activation-controlled mechanism without diffusion influence. Moreover, the presence of the inhibitor produced no significant potential shift compared to the blank solution, thereby classifying it as a mixed-type inhibitor that simultaneously affects both anodic and cathodic processes [25,26].

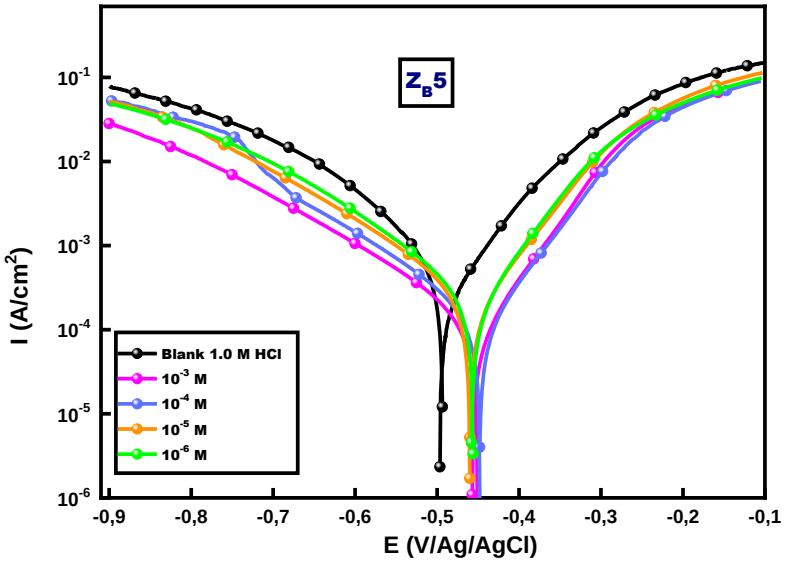

Figure 1. Polarization graphs for mild steel reprogrammed at 298 K in the studied environment before and after including various amounts of ZB5

Table 1. Electrochemical characteristics of mild steel were measured at 298 K before and after adding varying amounts of the investigated inhibitor to the media

Compounds	Conc. M	E_{corr} mV/Ag/AgCl	i_{corr} µA cm^{-2}	- β_c mV dec^{-1}	β_a mV.dec^{-1}	η_{PP} %
HCl 1.0M	--	-498	983	140	150	---------
Z_B5	10^{-3}	-450	147	119	105	85.04
	10^{-4}	-447	187	121	108	80.97
	10^{-5}	-460	320	130	118	67.44
	10^{-6}	-456	355	132	126	63.88

The analysis of the results in Table 1 shows that with increasing inhibitor concentration, i_{corr} values decline sharply. Hence, as the inhibitor concentration increases, the inhibitory efficiency "ηpp%" also rises, peaking at 85.04%. This result suggests that both products adsorb efficiently onto the metal surface's active sites, forming a protective film that reduces dissolution reactivity [27]. The inhibition efficiency (η) has been determined according to the following:

$$\eta_{pp} = [(i^0_{corr} - i_{corr}) / i^0_{corr}] \times 100 \quad (10)$$

Where, $i°_{corr}$ and i_{corr} indicate the corrosion current density before and after adding the chemical inhibitor.

The absolute values of E_{corr} decrease as ZB5 concentration increases, suggesting a shift in the corrosion potential. It may be inferred that ZB5 functions as a mixed-type inhibitor, as these values are lower than ±85 mV compared to the corrosion potential of the free combination. With these mixed-type inhibitors, mild steel rusts less in a 1.0 M HCl solution because the anodic (metal oxidation) and cathodic (oxygen or proton reduction) processes occur more slowly [28,29].

EIS measurements

To determine and collect data on the protection mechanism (charge transfer, diffusion, and adsorption), EIS measurements were performed. Figure 2 displays the Nyquist (2a) and Bode (2b) curves for the electrochemical characteristics of mild steel in "1.0 M HCl" at 298 K in the absence and presence of different amounts of ZB5.

The Nyquist plot in the presence of an inhibitor, as shown in Figure 2a, has a more pronounced arc diameter than that seen for the blank solution. The development of an inhibitive coating on the metallic surface, which slows down the corrosion process, is the most plausible explanation. The fact that each graph shows only one capacitive loop indicates that the charge-transfer process is primarily responsible for controlling the corrosion response [30]. Incomplete semicircles was obtained in the Nyquist spectra. This is most likely caused by various non-uniformities or rough electrode surfaces [31]. The Bode magnitude and phase plots, shown in Figure 2b, provide a clearer visual aid by referencing an equivalent circuit with a single constant phase element at the metal-environment contact. As the concentration of the molecules increases, so does the phase angle and the Bode graph. This suggests that the adsorption capacity of the inhibitor particles on the mild steel surface determines their protective capacity [32]. The model chosen to simulate the Niquist diagrams is shown in Figure 3 (equivalent circuit). Solution resistance (R_s), parallel constant phase element (CPE) ((Q_{dl}, n_{dl}) or (C_{dl}, n_{dl})), and a charge transfer resistance made up this electrical circuit (R_{ct}). As a result, all experimental data fit well in the existence and absence of quinazoline derivatives. The expression denotes the impedance function of the CPE [33]:

$$Z_{CPE}=1/Q(j\omega)-n_{dl} \quad (11)$$

Where, Q represents the CPE's magnitude, j stands for an imaginary number ($j^2 = -1$), and w represents the angular frequency. n_{dl}, the deflection parameter, denotes a phase shift ($-1 \leq n_{dl} \leq +1$). The CPE stands for a pure resistor if $n_{dl} = 0$, an inductor if $n_{dl} = 1$, and a pure capacitor if ndl = 1. Moreover, the following Equation has been used to determine the double-layer capacitances, C_{dl}, for a circuit that incorporates a CPE [33]:

$$C_{dl} = Q\,(2\pi\omega_{max})n_{dl}{}^{-1} \quad (12)$$

Where, ω_{max} ($\omega_{max} = 2\pi f_{max}$) & f_{max} are frequencies at the highest value of the imagined section of the impedance profile.

Table 2 summarizes the electrochemical parameters obtained for the ZB5 compound, including Rs, Rct, Q, ndl, and ηimp (%). The results show that Rct values increase progressively with concentration, reaching a maximum of 202.2 $\Omega\cdot cm^2$ at 10^{-3} M. Likewise, ndl values are consistently higher than those of the blank solution and rise with increasing concentration. These observations confirm that the inhibitor molecules adsorb effectively onto the steel surface, forming a stable protective layer [34].

The inhibition efficiency of the compound increases with concentration, from 56.14% at 10^{-6}M to 82.83% at 10^{-3}M. This further confirms that the protective film formed by the quinazolinone molecules on the electrode surface becomes denser, effectively shielding the metal from localized corrosion caused by chloride ions [35].

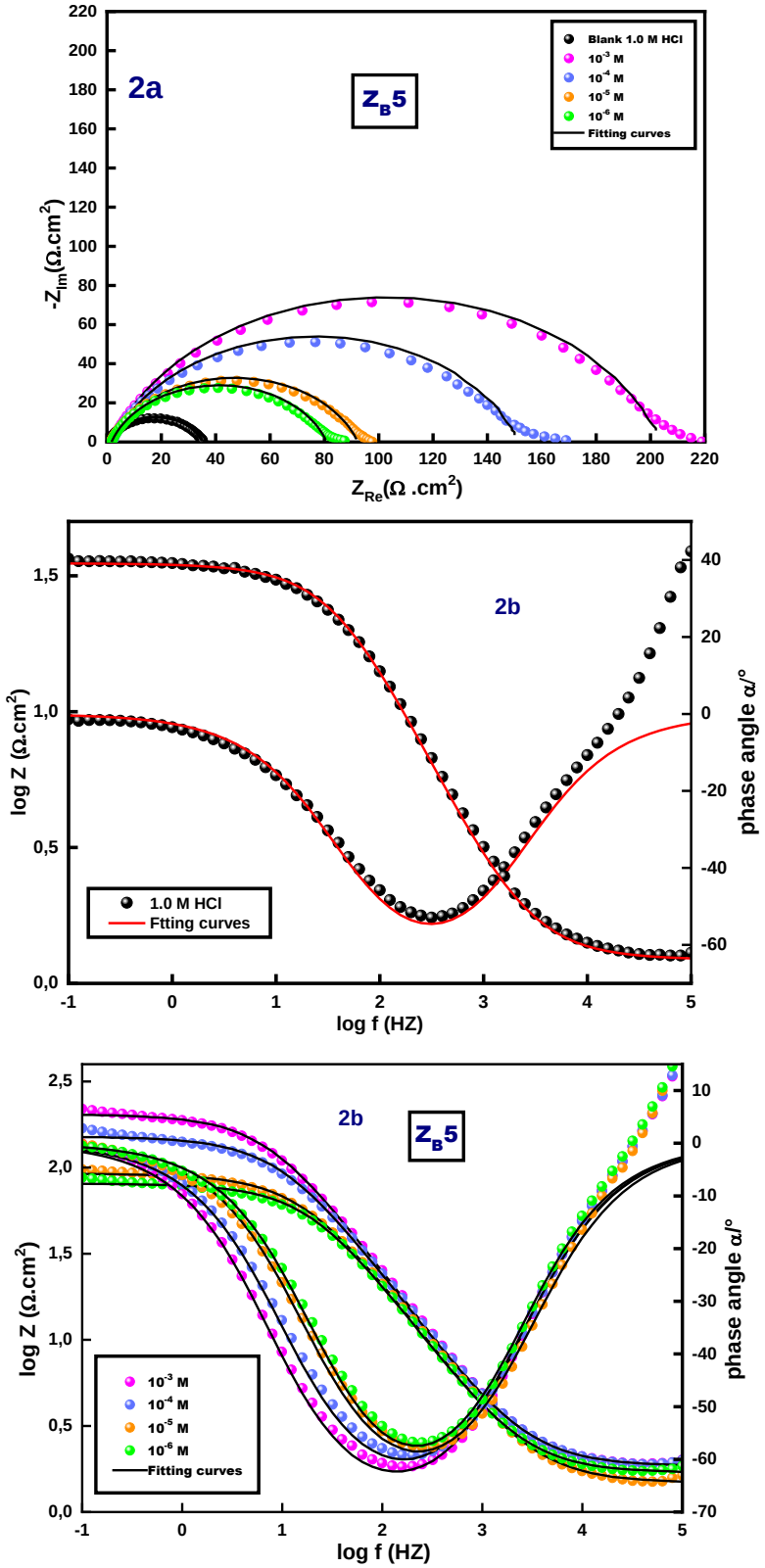

Figure 2. The EIS results for mild steel corrosion in 1.0 M HCl solution, with and without the ZB5 inhibitor, including Nyquist impedance graphs (2a) and Bode angle graphs (2b)

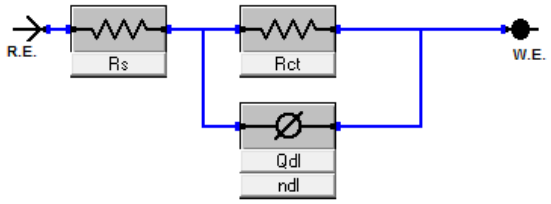

Figure 3. Corresponding circuits fitting with experimental impedance data

Table 2. Electrochemical impedance parameters for the inhibitory activity of mild steel were determined at 298 K in 1.0 M HCl solution before and after adding various quantities of ZB5

	Conc. (M)	R_s (Ω cm^2)	R_{ct} (Ω cm^2)	Q (μF. Sn^{-1})	n_{dl}	θ	ηimp %
HCl 1 M	-	1.12	34.7	419	0.773	-	-
	10-3	1.849	202.2	222	0804	0.8283	82.83
ZB5	10-4	1.835	149.7	245	0.794	0.7682	76.82
	10-5	1.469	90.81	268	0.796	0.6178	61.78
	10-6	1.687	79.13	258	0.704	0.5614	56.14

Adsorption isotherm

In corrosion inhibition, adsorption isotherms help explain the interactions between inhibitor molecules and the metal surface. They provide insights into the nature of the adsorption process, whether physical (physisorption) or chemical (chemisorption).

For the adsorption of organic inhibitors on mild steel, various isotherm models are commonly used, including the Langmuir, the Freundlich, and the Temkin isotherms. The criterion for selecting the best adsorption isotherm was the value of the regression coefficient (R2) that was closest to unity for the Langmuir adsorption isotherm model. According to this model, the degree of surface coverage (θ) is related to the inhibitor concentration (Cinh) by the following Equation [36]:

$$\frac{Cinh}{\theta} = \frac{1}{Kads} + Cinh \quad (13)$$

Where, θ is the surface coverage (calculated from inhibition efficiency), Cinh is the inhibitor concentration, and Kads is the adsorption equilibrium constant.

The plot of the Langmuir adsorption isotherm (Cinh/θ vs. Cinh) for corrosion of mild steel in an environment of 1.0 M HCl is presented in Figure 4.

The high regression coefficient values (R^2 = 0.9999 for Z5) confirm the appropriateness of this model. From the adsorption constant (Kads), the values of "ΔG°ads" were calculated using the following Equation (14) [37]:

$$\Delta Gads = -RT \ln (55.5 * Kads) \quad (14)$$

Where, RR denotes the universal gas constant, 55.55 represents the molar concentration of water in solution (mol L^{-1}), and TT is the absolute temperature (K).

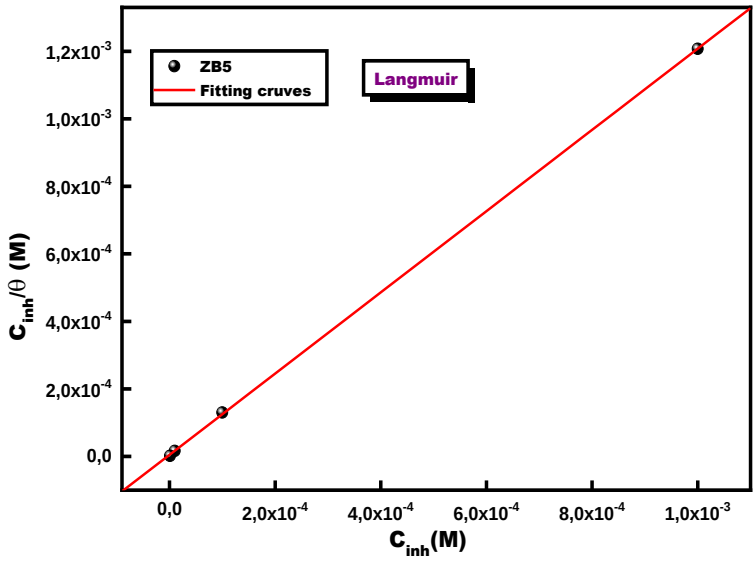

Figure 4. Langmuir adsorption curves for different quinazolinone derivatives on mild steel in 1.0 M HCl media at 298 K

Table 3. Thermodynamic parameters obtained for the adsorption of ZB5 on mild steel in 1.0 M HCl at 298 K using the Langmuir adsorption isotherm

Inhibitor	Kads (L/mol)	R^2	ΔGads (KJ/mol)
ZB5	212907.74	0.9999	-40.32

Generally speaking, the values of Kads and ΔGads can serve as a basis for evaluating the adsorption capacity of quinazolinone molecules on metal surfaces. The higher value of Kads, the inhibitor molecule, and the metal surface, will generate stronger interactions [38]. The result shows that the Kads of ZB5 is 212907.74 L/mol, indicating a strong bond between the metal and the inhibitor. The inhibition is absorbed spontaneously, as evidenced by the negative Gads readings [39]. It is well established that adsorption of organic molecules onto steel surfaces generally occurs via two primary mechanisms: physisorption and chemisorption. Physisorption, characterized by electrostatic interactions between charged inhibitor molecules and the metal surface, is typically inferred when ΔGads values are equal to or less than −20 kJ·mol^{-1}. In contrast, chemisorption is assumed when ΔGads values are equal to or greater than −40 kJ·mol^{-1}, reflecting charge sharing or electron transfer from the inhibitor molecules to the iron atoms (Table 3) [40]. Given that the ΔGads value in this study is close to −40 kJ·mol^{-1}, it can be inferred that the ZB5 compound undergoes spontaneous chemisorption onto the iron surface.

Temperature effect and activation parameters

By analyzing corrosion rate trends at different temperatures, typically using electrochemical methods, an inhibitor's thermal stability and effectiveness in mitigating corrosion can be assessed across various temperature ranges [41]. The effect of temperature on the corrosion rate of Mild steel in 1.0 M HCl, both with and without 10^{-3} M ZB5 inhibitor, was investigated at temperatures ranging from 298 to 328 K. The

polarization curves and parameters resulting from this study are shown in Figure 5 and summarized in Table 4, respectively. The study shows that current density increases with rising temperature for mild steel in 1 M HCl, both in the absence and in the presence of inhibitors. This can be attributed to accelerated chemical processes, indicating that the corrosion rate of mild steel is temperature-dependent [42]. Furthermore, the inhibitory efficacy of the product decreases with increasing temperature, suggesting that the inhibitor molecule adsorbs onto the steel surface via either chemical adsorption or weak chemical bonds [43]. These findings highlight the sensitivity of the inhibition process to temperature variations.

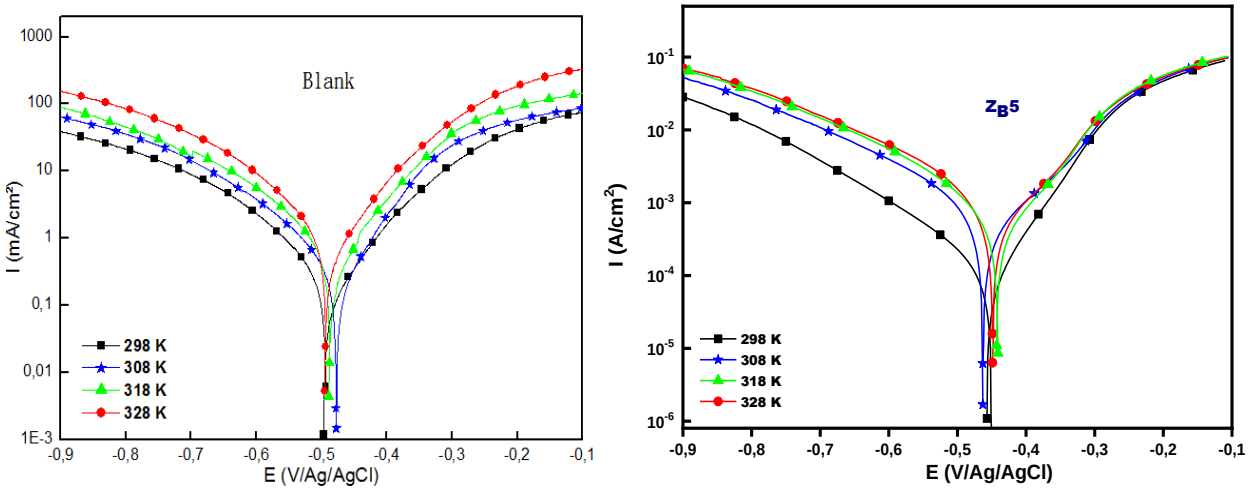

Figure 5. Mild steel's polarization curves in 1.0 M HCl in the presence and absence of inhibitors at various temperatures

Table 4. Polarization plot parameters of mild steel in 1.0 M HCl containing '10^{-3} M' of ZB5 at various temperatues

Compounds	Temperature (K)	E_{corr} mV/Ag/AgCl	i_{corr} µA cm^{-2}	$-\beta_c$ mV dec^{-1}	β_a mV dec^{-1}	E%
Blank	298	-498	983	140	150	----
	308	-477	1200	184	112	----
	318	-487	1450	171	124	----
	328	-493	2200	161	118	----
ZB5	298	-450	147	119	105	85.04
	308	-464	320	123	117	73.33
	318	-441	450	140	126	68.69
	328	-448	686	156	130	68.81

The Arrhenius Equation and activation energy calculations are commonly applied to assess the impact of temperature on corrosion rates and inhibitor efficiency. The kinetic and thermodynamic parameters, including apparent activation energy (E_a), activation enthalpy (ΔH_a), and activation entropy (ΔS_a) for dissolving mild steel in 1.0 M HCl, both in the absence and presence of 10-3 M ZB5 at temperatures ranging from 298 to 328 K, are shown in Figure 6 and Table 5. These activation parameters were derived using the Arrhenius Equation as the foundational model for the calculations [44]:

$$i_{corr} = Ae\text{-}E_a/RT \quad (15)$$

Taking the logarithm from both sides of the Arrhenius Equation, Equation (16) is obtained:

$$\text{Ln } i_{corr} = \text{Ln } A - E_a/RT \quad (16)$$

The transition state Equation was used to determine the variation in enthalpy (ΔH_a) and entropy (ΔS_a) for producing the activated complex in the state of transition [45]:

$$\ln\left(\frac{icorr}{T}\right) = \left[\ln\left(\frac{R}{hNa}\right) + \left(\frac{\Delta Sa}{R}\right)\right] - \Delta Ha/RT \quad (17)$$

Where, i_{corr} is the corrosion current density, A denotes pre-exponential factor, h is Planck's constant, Na indicates Avogadro's number, E_a is the apparent activation energy, R denotes gas constant (R = 8.314 J mol^{-1}. K^{-1}), and T is the absolute temperature.

The plots of $\ln(i_{corr})$ and $\ln(i_{corr}/T)$ as a function of 1000/T, shown in Figure 6, display a straight line with a slope corresponding to $(-E_a/R)$. The activation energy (E_a) values were determined from the slope of this line and are presented in Table 5.

The higher activation energy (E_a) observed in the solution containing 10^{-3} M of ZB5, compared to the uninhibited medium, indicates that the quinazolinone derivative is physically adsorbed onto the mild steel surface. This behavior can be attributed to the formation of a thin protective film that increases the energy barrier to corrosion. The presence of this adsorbed inhibitor layer effectively hinders charge-transfer reactions at the steel interface, thereby reducing the oxidation rate. Overall, these findings confirm that ZB5 enhances the corrosion resistance of mild steel by making the corrosion process more difficult under the tested conditions [46].

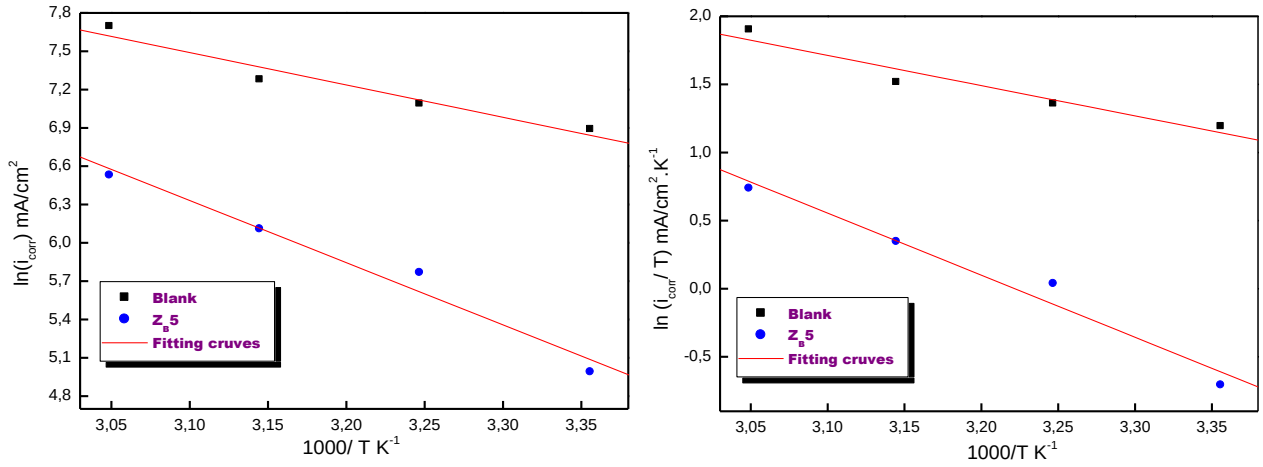

Figure 6. Straight recomposition of ln (i_{corr} /T) vs. the opposite of the temperature employed to collect the activation parameters of ZB5

Table 5. Activation parameters for mild steel in 1.0 M HCl solution in the absence and presence of ZB5 inhibitor

	E_a (KJ/mol)	ΔH_a (KJ/mol)	ΔS_a (J/mol.K)
Blanc	21.0	18.5	-126.0
ZB5	40.46	37.87	-75.62

Data also show that the enthalpy of activation (ΔH_a) obtained in the presence of ZB5 is higher than that of the solution-free, indicating an endothermic corrosion process between the compound (ZB5) and Fe in an acidic environment [47]. Furthermore, the entropy change (ΔS_a) decreases upon addition of ZB5, indicating a less disordered state, as the complex is active during the speed establishment phase.

Surface characterization

SEM/EDS analysis

The surface morphology of mild steel was examined by SEM after 6 hours of immersion in 1.0 M HCl, both in the absence and presence of 10^{-3} M ZB5. The untreated sample exposed to the uninhibited solution (Figure 7a, BLK) exhibited severe surface damage and pronounced roughness caused by the corrosive medium. In contrast, the specimen treated with the film-forming ZB5 solution (Figure 7b) displayed a markedly smoother and less deteriorated surface, confirming the effectiveness of the protective layer. These results demonstrate that adsorption of the quinazolinone derivative onto the mild steel surface substantially mitigates corrosive attack. To validate the elemental composition of the film formed on the steel surface, energy-dispersive X-ray spectroscopy (EDS) analysis was conducted. Figure 7 (c and d) shows the characteristic peaks of C, O, Cl, and Fe detected before and after immersion in 1.0 M HCl containing 10^{-3} M ZB5. The corresponding elemental percentages on the steel electrode are summarized in Table 6.

The ZB5 spectrum shows a significant reduction in signals from C and O relative to the untreated sample, while Fe content increases. This indicates that the quinazolinone derivative is well adsorbed onto the metallic surface, forming a barrier layer that resists corrosion.

FTIR analysis

Fourier Transform Infrared (FTIR) spectroscopy was used to examine the chemical composition changes on the surface of mild steel after 6 hours of immersion in the treated and untreated samples (Figure 8). This technique allows the identification of functional groups present and helps analyze the interaction between inhibitor molecules and the metal surface [48,49].

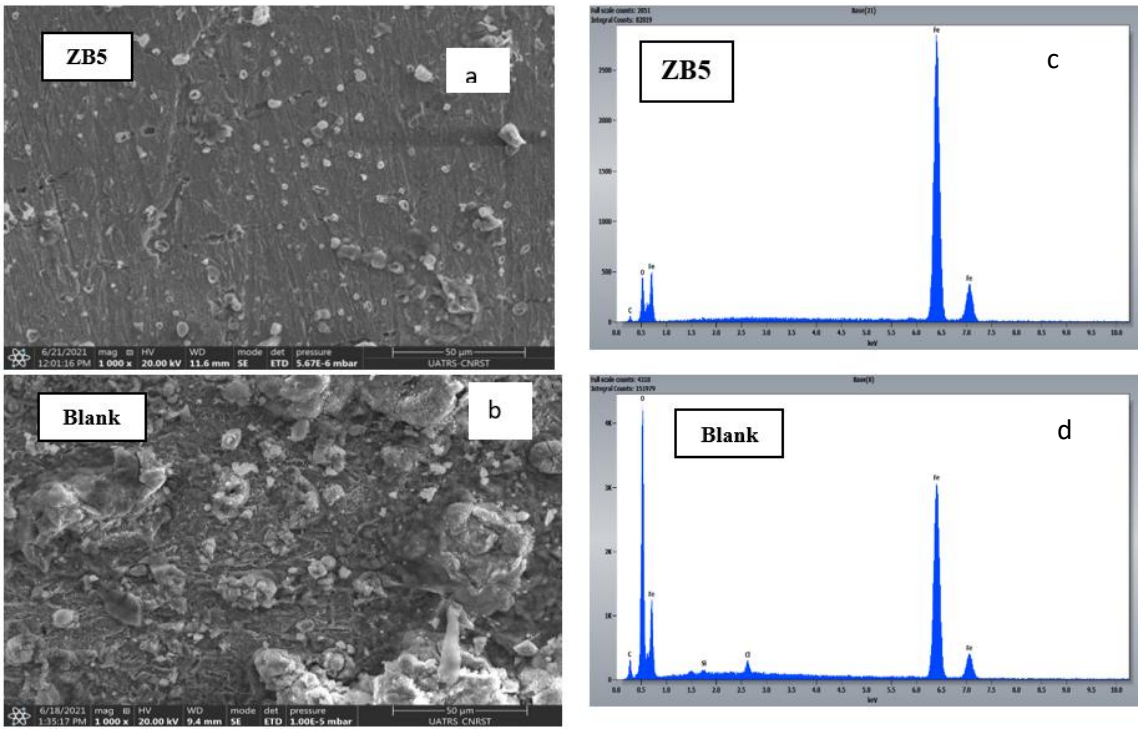

Figure 7. SEM micrographs (a, b) & EDS spectra (c, d) of the mild steel after 6 H immersion in 1.0 M HCl before and after adding 10-3 M of ZB5

Table 6. Compositions of the mild steel surface tested by EDS analysis

Elements	Blank	ZB5
C	7.62	4.21
O	27.95	16.2
Fe	62.89	79.58
Cl	1.04	--
Si	0.35	--

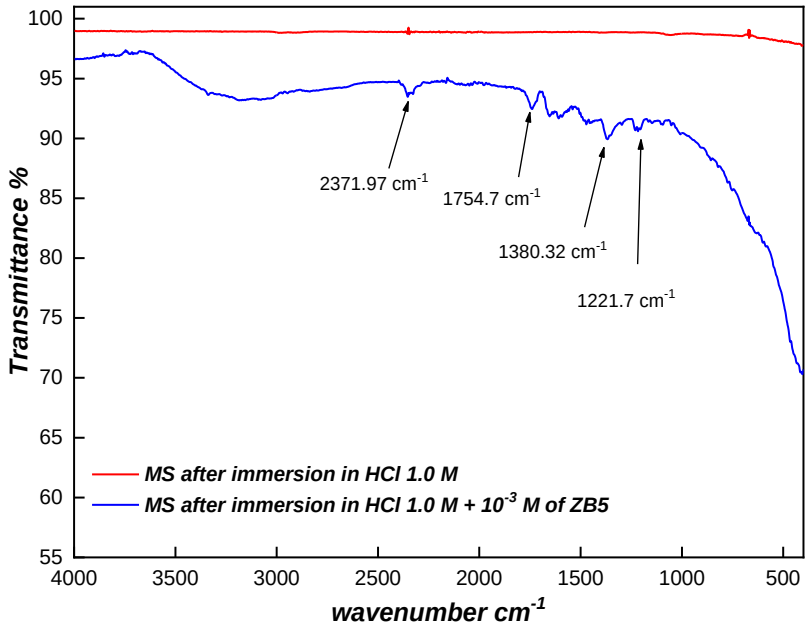

Figure 8. FT-IR spectrum of the mild steel surface layer before and following the introduction of ZB5

The FT-IR spectrum (Figure 8) of the solution containing the ZB5 inhibitor shows several characteristic peaks at specific wave numbers, corresponding to the different molecular vibrations of the functional groups present in the inhibitor. These peaks confirm the presence of ZB5 adsorbed on the Mild steel surface, indicating an interaction occurred between the inhibitor molecules and the metal surface.

In contrast, in the absence of ZB5, these peaks disappear from the spectrum, suggesting that there is no significant adsorption of other compounds or the formation of a protective film on the surface. This indicates that the ZB5 inhibitor protects against corrosion by forming a barrier on the mild steel surface, reducing its direct exposure to the aggressive HCl solution. This protective layer limits corrosion by blocking active sites on the steel surface, thereby enhancing resistance to the corrosive attack.

X-ray analysis

Figure 9 shows the XRD diffractograms. The results for the untreated solution reveal Fe_3O_4 and Fe_2O_3 peaks (iron oxides) at $2\theta = 29.40°$ and 65°, respectively. These iron oxides form as a result of the corrosive attack by the acidic solution on the steel surface. The formation of these oxides is a clear sign of ongoing corrosion, as the steel reacts with hydrochloric acid, producing these compounds.

In contrast, incorporation of the ZB5 inhibitor resulted in a significant reduction in the peak intensities of the iron oxides (Fe_3O_4 and Fe_2O_3). This reduction suggests that the formation of these oxides has been inhibited, indicating that

the steel surface has been effectively isolated and protected from the aggressive acidic environment by a protective layer formed by ZB5. This protective film likely blocks the active corrosion sites on the steel surface, preventing further oxidation reactions and the formation of iron oxides [43].

Solution analysis by ICP-OES

Inductively coupled plasma optical emission spectrometry (ICP-OES) enables the accurate determination of the elemental composition and concentration of dissolved iron ions in mixtures with and without inhibitors. Table 7 presents the concentration values of Fe^{2+} ions found in a 1.0 M HCl solution alone, as well as after the addition of different concentrations of ZB5.

The results show that the concentration of Fe^{2+} ions in the solution decreases as the inhibitor concentration increases. For ZB5, the concentration of Fe^{2+} ions drops from 1,152 mg/L in the control solution (without inhibitor) to 590.3-175.9 mg/L as the inhibitor concentration increases from 10^{-6} M to 10^{-3} M.

These findings demonstrate that the studied inhibitor rapidly inhibits steel dissolution. The higher the inhibitor concentration, the lower the amount of Fe^{2+} ions released into the solution. This significant reduction in the concentration of Fe^{2+} ions in the corrosive solution indicates that the inhibitors form a protective barrier on the steel surface, thus preventing the dissolution of the metal in hydrochloric acid [41]. This protective mechanism, through the adsorption of inhibitors on the metal surface, is therefore essential for extending the durability and resistance of steel in corrosive environments.

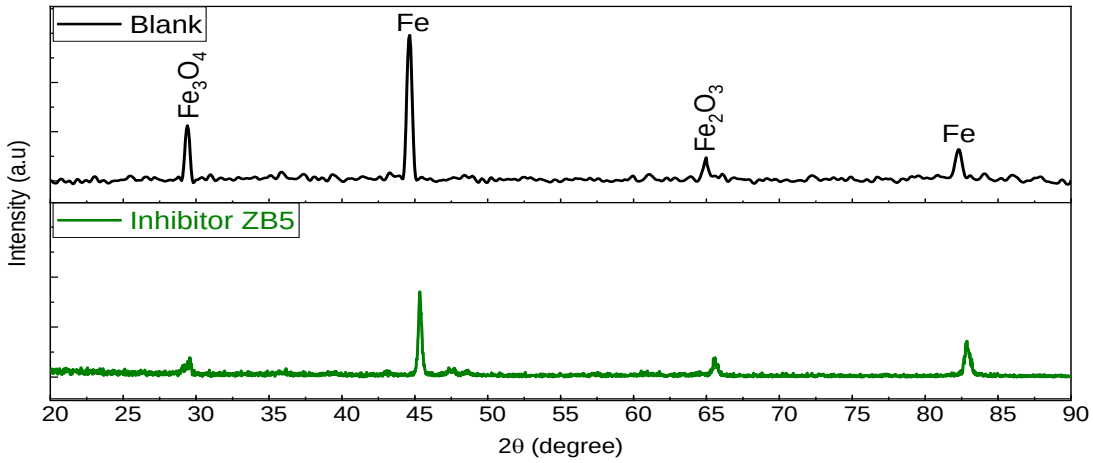

Figure 9. Diffractograms of mild steel surface after six hours of immersion in 1.0 M HCl (with and without 10-3 M of ZB5)

Table 7. Concentration of Fe^{2+} ions in 1.0M HCl with and without the presence of various quantities of ZB5

Compounds	Conc. (M)	Conc. Fe^{2+} ions (mg/L)
HCl 1 M	--	1152
ZB5	10-3	175.9
	10-4	274.9
	10-5	385.1
	10-6	590.3

DFT calculation

Figure 10 illustrates the optimized geometry and the distribution of the frontier orbitals of the molecule in its two states: the neutral form in the gas phase and the protonated form in the aqueous phase. In both configurations, the highest occupied molecular orbital (HOMO) and the lowest unoccupied molecular orbital (LUMO) are primarily localized on nitrogen and carbon atoms. This orbital distribution is particularly significant as it promotes the adsorption of the molecule onto a metallic surface. The nitrogen atoms, especially those with lone pairs of electrons, interact effectively with the active sites of the metallic surface [17]. Localizing orbitals in specific regions of the molecule increases the likelihood of forming chemical or physical bonds with the metallic atoms, thereby enhancing the efficiency of the corrosion-inhibition process. This interaction is especially pronounced in the gas phase, where the neutral form of the molecule exhibits enhanced adsorption characteristics due to electrostatic effects and increased polarity.

The energy values of the highest occupied molecular orbital (E_{HOMO}) and the lowest unoccupied molecular orbital (E_{LUMO}) were used to calculate the energy gap ($\Delta E = E_{LUMO} - E_{HOMO}$) and to analyze interactions. Various chemical reactivity descriptors, such as absolute electronegativity (χ), hardness (η), softness (σ), and electrophilicity (ω), were evaluated for the neutral form in the gas phase and the protonated form in the aqueous phase. These results are summarized in Table 8. According to the frontier molecular orbital (FMO) theory, a molecule's ability to exchange electrons is determined by the energy levels of its E_{LUMO} and E_{HOMO} orbitals. A high E_{HOMO} indicates a strong tendency for the inhibitor to donate electrons to the metal's vacant orbitals, enhancing adhesion to the metal surface and improving its protective efficiency [5]. Conversely, a low E_{LUMO} indicates the inhibitor's superior ability to accept electrons from the metal, further contributing to its effectiveness [18].

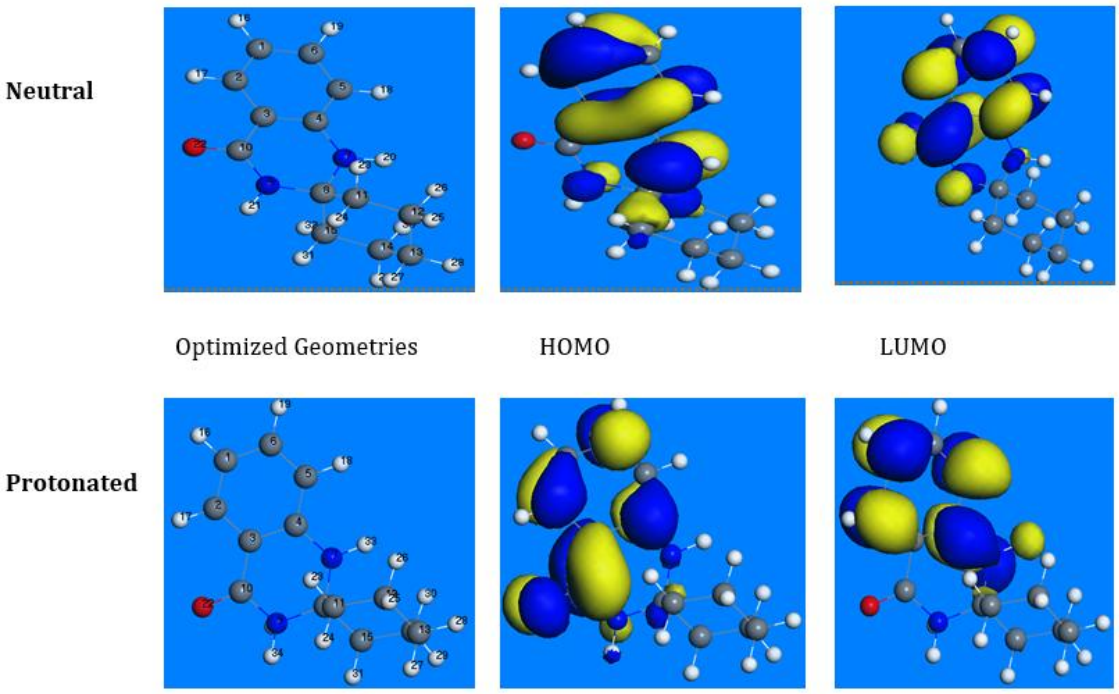

Figure 10. Optimized geometries and frontier orbital density distributions of ZB5 molecule

The molecular processes involved in chemical reactions are comparable to those in adsorption, in which only the HOMO and LUMO orbitals near the Fermi level participate of the substrate. Figure 11 illustrates the energy levels of the frontier orbitals for the neutral and protonated forms of the inhibitor, along with their relationship to the Fermi level. The HOMO orbitals of the molecule are closer to the Fermi level of Fe (-5.177 eV) than the LUMO orbitals, which is particularly notable for the neutral form. This proximity facilitates the migration of electrons from the HOMO orbitals to the metallic surface [19,20]. Conversely, electron transfer from the metal to the molecule's LUMO orbitals is less likely due to a significant energy gap. The molecule acts as an electron donor, accumulating electrons on the iron surface until equilibrium is established.

Based on the quantum-chemical parameters presented in Table 8, the neutral form of the inhibitor appears to be the most stable. However, this form has a relatively large energy gap and high hardness. Due to its low reactivity, the neutral form does not interact optimally with the metal surface, thereby limiting its potential to inhibit corrosion in acidic solutions such as HCl. In contrast, the protonated form of the inhibitor exhibits characteristics that significantly enhance its effectiveness as a corrosion inhibitor. The energy gap of this form is considerably lower, indicating greater chemical reactivity.

Furthermore, the protonated form has reduced chemical hardness, making it more flexible and able to interact with the metal surface [2,21-23]. Its higher softness enables better interactions with the surface's active sites, promoting the adsorption of the molecule [24]. Additionally, the increased electronic transfer in the protonated form suggests an improved ability to donate electrons to the metal surface, strengthening adsorption and corrosion inhibition in an acidic environment containing HCl [16,25]. These properties make the protonated form much more effective in protecting metal surfaces from corrosion, particularly under acidic conditions.

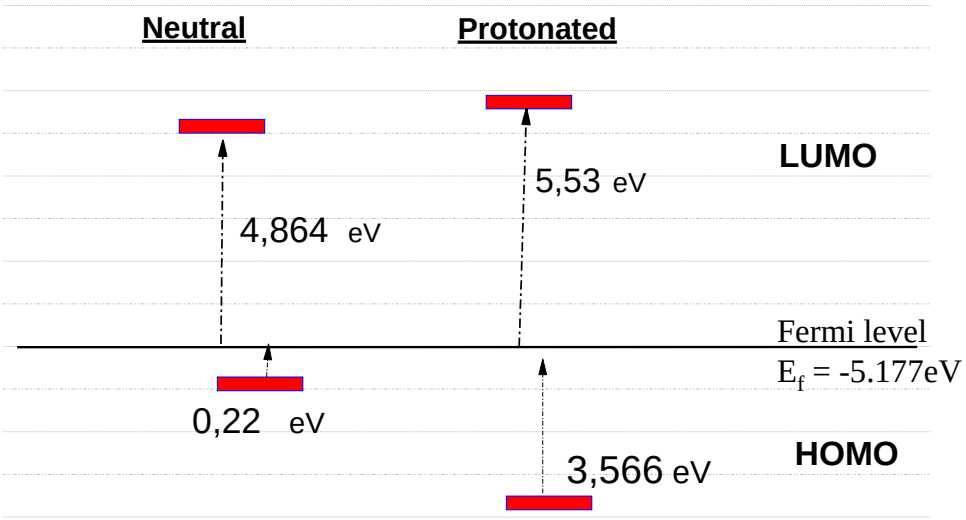

Figure 11. The energy gaps of the orbitals relative to the Fermi level were calculated using the B3LYP/6-311G+(d,p) method

Table 8. Quantum chemical parameters from DFT calculation

	Neutral	Protonated
ELUMO (ev)	-0.313	0.353
EHOMO (ev)	-4.957	-1.611
ΔE(eV)	4.643	1.964
η(eV)	2.321	0.982
S (eV)	0.430	1.017
χ(eV)	2.635	0.628
ΔN110	0.470	2.133
ω	4.643	1.964

The local reactivity indices of the studied inhibitors were calculated and are illustrated in Figure 12. It is widely recognized that when the double local descriptors ($f_k^2\ \Delta S_k\ and\ \Delta\omega_k$) show values below zero, this indicates a high probability of electrophilic attack at site k due to its high electron density. Conversely, when these descriptors are above zero, a nucleophilic attack is favored, suggesting that the site has low electron density and thus attracts nucleophiles [26,27]. Figure 12 reveals that the two analyzed forms have several active centers. Some of these centers show local descriptor values below zero, suggesting a high probability of electrophilic attack, while others show values above zero, favoring nucleophilic attack. These observations indicate that the molecule primarily acts via a back-donation mechanism, thereby enhancing adsorption and improving corrosion-inhibition efficiency. The carbon (C), oxygen (O), and nitrogen (N) atoms play a key role in this process, as they are often the active sites for electrophilic and nucleophilic interactions. Their ability to form strong bonds with the metallic surface is crucial for ensuring the optimal adsorption and effective corrosion inhibition.

MC simulation

Figure 13 shows the equilibrium adsorption geometries of the studied inhibitor molecule in both its neutral and protonated states in a solution containing 7 H^+ ions, 7 Cl^- ions, and 700 water (H_2O) molecules. This setup allows for a detailed analysis of the interaction between the inhibitor molecules and the metallic Fe(110) surface. As shown in Figure 13, the inhibitor molecule aligns parallel to the metallic surface, thereby optimizing the interactions between its functional groups and the surface atoms. These interactions are primarily governed by the carbon, nitrogen, and oxygen atoms in the molecular structure of the inhibitor. In the protonated state, the interaction is generally stronger, as the positive charge enhances electrostatic attraction to the metallic surface. Conversely, in the neutral state, the interactions are dominated by van der Waals forces and coordination interactions involving electron-donating atoms, such as nitrogen and oxygen [24]. These findings confirm that the effectiveness of the inhibitor molecules depends strongly on their orientation and on the specific interactions between their functional groups and the metallic surface.

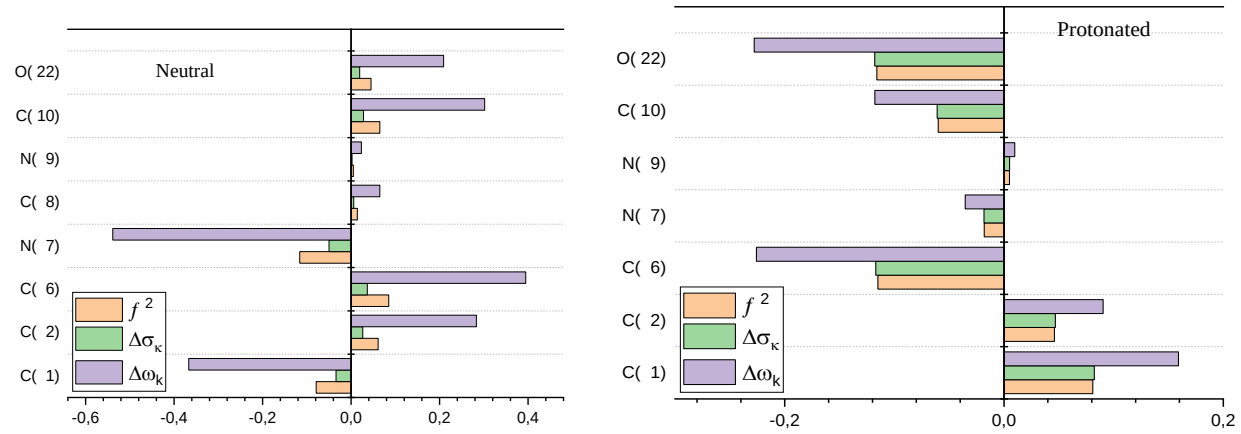

Figure 12. Graphical display of the local dual descriptors (Δfk, Δσ, and Δω) of ZB5

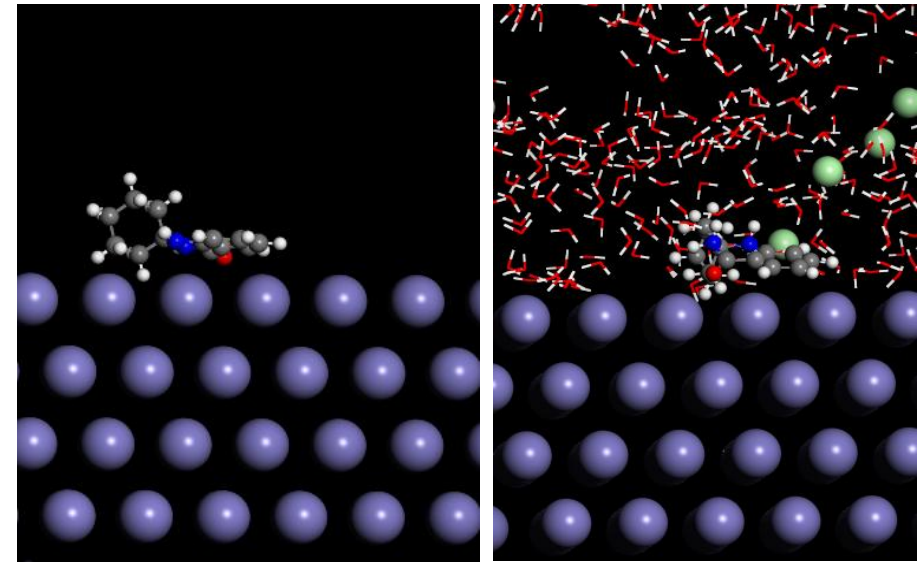

Figure 13. The equilibrium adsorption configurations of ZB5 on the Fe (110) surface

After optimization, Table 9 presents the estimated adsorption energies of the molecules on the Fe (110) surface for the gas-phase and aqueous-phase protonated forms. The results show that both forms, protonated and neutral, exhibit more negative adsorption energies. This suggests more stable adsorption, which could enhance the effectiveness of these molecules as corrosion inhibitors, as more stable adsorption provides better surface protection against corrosion [28,29].

Inhibition mechanism for ZB5

The chemical structures of the inhibitor molecules and the type and charge of the metal generally play key roles in the mechanism of action of corrosion inhibitors on metal surfaces in acidic media. Based on the available data, the adsorption process of the compounds on the mild steel surface can be described as follows (Figure 13):

1) Studies conducted in HCl medium showed that the metal surface becomes positively charged [30]. The tested compound, containing nitrogen and oxygen atoms, undergoes facile protonation in this medium. In addition, the positively charged CS surface facilitates the adsorption of chloride ions (Cl^-), serving as a bridge between the protonated SB5 molecules and the CS surface. This bridging effect enhances the electrostatic interactions among the components, consistent with a physisorption mechanism (Figure 14).
2) As shown by the previously mentioned results, chemisorption can also inhibit corrosion. The presence of electron-rich rings and heteroatoms (N and O) facilitates the transfer of electrons from SB5 molecules to the electron-deficient orbitals of iron. In this mechanism, the non-shared electron pairs of nitrogen and oxygen atoms can donate their electrons to the vacant iron orbitals (chemisorption), and donor-acceptor interactions can occur between the π-electrons of the phenolic rings and the vacant iron orbitals (retro-donation) [17].

Table 9. Adsorption energy (kJ mol^{-1}) of the three inhibitory molecules studied on the iron surface under solvation conditions

Total energy (kJ/mol)	Adsorption energy (kJ/mol)
SB5 /Fe (110)	
-604.22	-212.6
SB5 /Fe (110) /7 H3O+/7 Cl-/700 H2O	
-50295.31	-109164.17

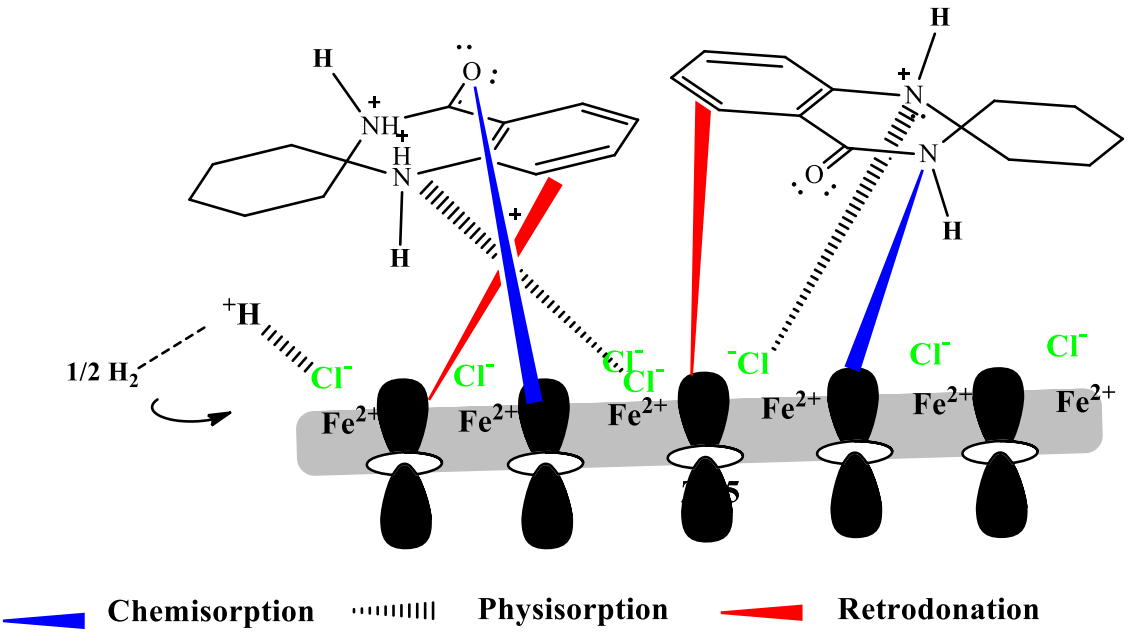

Figure 14. Corrosion inhibition scheme of mild steel by SB5

Conclusion

In conclusion, the quinazolinone derivative ZB5 demonstrated remarkable efficiency as a corrosion inhibitor for mild steel in acidic environments, achieving up to 82.83% protection at a concentration of 10^{-3} M. The adsorption behavior of ZB5 followed the Langmuir isotherm model, and surface analyses (SEM/EDS, XRD, FTIR, and ICP-OES) confirmed the formation of a protective layer on the steel surface. Furthermore, theoretical studies using DFT and MC simulations provided strong evidence linking the electronic and adsorption properties of ZB5 to its experimental inhibition performance. These comprehensive findings highlight ZB5's potential as a promising corrosion protection candidate in aggressive acidic media. Future work could explore its long-term stability, scalability, and performance under industrial conditions to further validate its practical applicability.

Acknowledgement

The authors would like to gratefully acknowledge the Euromed University of Fez for its support and contribution to this research.

Disclosure Statement

No potential conflict of interest was reported by the authors in this work.

ORCID

Hind Malki:
https://orcid.org/0009-0004-7687-8052
Otmane Kharbouch:
https://orcid.org/0000-0001-6577-6828
Fatima Hamouche:
https://orcid.org/0000-0002-2154-6112
Nadia Dkhireche:
https://orcid.org/0009-0008-7127-5286
Khalil El Mabrouk:
https://orcid.org/0000-0002-7097-0737
Fatima Elhajri:
https://orcid.org/0009-0003-1846-898X
Zakaria Benzekri:
https://orcid.org/0000-0002-6039-6073
Said Boukhris:
https://orcid.org/0000-0001-9541-4318

References

[1] Soliz, A., Zamora, P.P., Muena, J.P., Bieger, K., Haribabu, J., Landaeta, E., Arulraj, A., Mangalaraja, R.V. Experimental and DFT analysis of the concentration dependency of corrosion inhibition by a pyridine schiff base for mild steel in HCL solution. *Colloids and Surfaces A: Physicochemical and Engineering Aspects*, **2024**, 703, 135283.

[2] Singh, A., Ansari, K., Chauhan, D.S., Quraishi, M., Kaya, S. Anti-corrosion investigation of pyrimidine derivatives as green and sustainable corrosion inhibitor for N80 steel in highly corrosive environment: Experimental and AFM/XPS study. *Sustainable Chemistry and Pharmacy*, **2020**, 16, 100257.

[3] Landolt, D. Corrosion et chimie de surfaces des métaux (presses polytechniques et universitaires romandes). *Lausanne*, **1997**, 386–388.

[4] Lu, H., Ji, X., Ci, X., Zhu, H., Wang, Q., Zong, Y., Tian, H. Investigation of triazole derivatives as corrosion inhibitors on Q235 steel in NaCl solution: Experimental and theoretical studies. *Colloids and Surfaces A: Physicochemical and Engineering Aspects*, **2023**, 674, 131892.

[5] Kumar, B., Vashisht, H., Goyal, M., Kumar, A., Benhiba, F., Prasad, A.K., Kumar, S., Bahadur, I., Zarrouk, A. Study of adsorption mechanism of chalcone derivatives on mild steel-sulfuric acid interface. *Journal of Molecular Liquids*, **2020**, 318, 113890.

[6] Dariva, C.G., Galio, A.F. Corrosion Inhibitors: Principles, Mechanisms and Applications. Developments in Corrosion Protection. *Developments in corrosion protection*, **2014**, 16, 365-378.

[7] Fergachi, O., Benhiba, F., Rbaa, M., Ouakki, M., Galai, M., Touir, R., Lakhrissi, B., Oudda, H., Touhami, M.E. Corrosion inhibition of ordinary steel in 5.0 M HCL medium by benzimidazole derivatives: Electrochemical, UV–Visible spectrometry, and DFT calculations. *Journal of Bio-and Tribo-Corrosion*, **2019**, 5(1), 21.

[8] Hamzah, B.F., Al-Tamimi, E.O., Mhaibes, R.M. Synthesis of 4-Azo-3,5-substituted-1,2,4-triazole polymers and study of their applications. *Advenced Journal of Chemistry, Section A*, **2025**, 8(1), 65–79.

[9] Khan, G., Basirun, W.J., Kazi, S.N., Ahmed, P., Magaji, L., Ahmed, S.M., Khan, G.M., Rehman, M.A., Badry, A.B.B.M. Electrochemical investigation on the corrosion inhibition of mild steel by quinazoline schiff base compounds in hydrochloric acid solution. *Journal of Colloid and Interface Science*, **2017**, 502, 134–145.

[10] Aldana-González, J., Cervantes-Cuevas, H., Alfaro-Romo, C., Rodriguez-Clemente, E., Uruchurtu-Chavarin, J., Romero-Romo, M., de Oca-Yemha, M.M., Morales-Gil, P., Mendoza-Huizar, L.H., Palomar-Pardave, M., Experimental and theoretical study on the corrosion inhibition of API 5L X52 steel in acid media by a new quinazoline derivative. *Journal of Molecular Liquids*, **2020**, 320, 114449.

[11] Abulhail, A.N., Kadhum, M.Y. Experimental and theoretical studies of Schiff bases derived from 3,4-diamino pyridine as corrosion inhibitors for carbon steel N80 in acidic medium. *Advanced Journal of Chemistry, Section A*, **2025**, 8(2), 361–377.

[12] Malki, H., El Hassani, A.A., El Hamzi, S., Dkhirech, N., Forsal, I., Elhajri, F., Benzekri, Z., Benjelloun, A.T., Boukhris, S. Investigating quinazolinone derivatives as corrosion inhibitors for mild steel in 1.0 M HCl: Experimental insights, DFT calculations, and MC simulations. *Analytical and Bioanalytical Electrochemistry*, **2024**, 16, 568–594.

[13] Hmamou, D.B., Salghi, R., Zarrouk, A., Hammouti, B., Al-Deyab, S., Bazzi, L., Zarrok, H., Chakir, A., Bammou, L. Corrosion inhibition of steel in 1 M hydrochloric acid medium by chamomile essential oils. *International Journal of Electrochemical Science*, **2012**, 7(3), 2361–2373.

[14] Fergachi, O., Rbaa, M., Ouakki, M., Touir, R., Benhiba, F., Lakhrissi, B., Oudda, H., Touhami, M.E. Comparative study of corrosion inhibition effect for ordinary steel in HCL 5.0 M. *Materials Research*, **2022**, 25, e20210543.

[15] Tazouti, A., Errahmany, N., Rbaa, M., Galai, M., Rouifi, Z., Touir, R., Zarrouk, A., Kaya, S., Touhami, M.E., El Ibrahimi, B., Erkan, S. Effect of hydrocarbon chain length for acid corrosion inhibition of mild steel by three 8-(n-bromo-R-alkoxy) quinoline derivatives: experimental and theoretical investigations. *Journal of Molecular Structure*, **2021**,1244, 130976.

[16] Ayati, N., Khandandel, S., Momeni, M., Moayed, M.H., Davoodi, A., Rahimizadeh, M. Inhibitive effect of synthesized 2-(3-pyridyl)-3, 4-dihydro-4-quinazolinone as a corrosion inhibitor for mild steel in hydrochloric acid. *Materials Chemistry and Physics*, **2011**, 126(3), 873–879.

[17] El Amri, A., Azogagh, M., Sayed, R., El Amri, A., Er-rahmany, N., Hamouche, F., Hsissou, R., Dkhireche, N. Synthesis characterisation and analysis of the corrosion resistance of a new epoxy resin onto mild steel in the presence of hydrochloric acid: Practical and theoretical points of view. *Canadian Metallurgical Quarterly*, **2025**, 65(1), 1–21.

[18] Benzekri, Z., Anahmadi, H., Sibous, S., Ouasri, A., Souizi, A., Hassikou, A., Rhandour, A., Boukhris, S. Investigation of catalytic performance of Bis [hydrazinium (1+)] hexafluoridosilicate:(N2H5) 2SiF6 in synthesis of 2, 4, 5-triaryl-1H-imidazoles and 2, 3-dihydroquinazolin-4 (1H)-ones under Green conditions. *Inorganica Chimica Acta*, **2022,** 536, 120915.

[19] Hmada, A., Sayed, R., Hamouche, F., Errahmany, N., Anahmadi, H., Galai, M., Boukhris, S., Harcharras, M., Dkhireche, N. Enhancing corrosion resistance of mild steel in acid pickling bath: An investigation of new quinazoline derivatives by synthesis, electrochemical analysis EFM, surface analysis, AFM, DFT and molecular dynamics simulation. *Inorganic Chemistry Communications*, **2025**, 172, 113640.

[20] Geerlings, P., Fias, S., Boisdenghien, Z., De Proft, F. Conceptual DFT: Chemistry from the linear response function. *Chemical Society Reviews*, **2014**, 43(14), 4989–5008.

[21] Fukui, K., Yonezawa, T., Shingu, H. A molecular orbital theory of reactivity in aromatic hydrocarbons. *The Journal of Chemical Physics*, **1952**, 20(4), 722–725.

[22] Fuentealba, P., Cárdenas, C. On the analysis of the fukui function. *Chemical Reactivity,* **2023**, 1, 421–432.

[23] Muena, J.P., Zamora, P.P., Bieger, K., Soliz, A., Haribabu, J., Aguirre, M.J., Márquez, P., Quezada, D., Honores, J. Study of the reaction mechanism in hydrogen production using metal-free Schiff base as a catalyst. *Journal of Molecular Liquids*, **2023**, 391, 123207.

[24] Khudhair N.A., Al-Mousawi I.M.H., Ali M.I. DFT-quantum chemical and experimental studies of eco-friendly approach to corrosion inhibition of stainless steel 316L in body fluid solution by dexamethasone drug. *Advanced Journal of Chemistry, Section A*, **2024**, 7(6), 868-882.

[25] Naseri, E., Hajisafari, M., Kosari, A., Talari, M., Hosseinpour, S., Davoodi, A. Inhibitive effect of clopidogrel as a green corrosion inhibitor for mild steel; statistical modeling and quantum monte carlo simulation studies. *Journal of Molecular Liquids*, **2018**, 269, 193–202.

[26] Li, X., Deng, S., Xie, X. Experimental and theoretical study on corrosion inhibition of oxime compounds for aluminium in HCl solution. *Corrosion Science*, **2014**, 81, 162–175.

[27] Kissi, M., Bouklah, M., Hammouti, B., Benkaddour, M. Establishment of equivalent circuits from electrochemical impedance spectroscopy study of

corrosion inhibition of steel by pyrazine in sulphuric acidic solution. *Applied Surface Science*, **2006**, 252(12), 4190-4197.

[28] Gonçalves, R.S., Azambuja, D.S., Lucho, A.M.S. Electrochemical studies of propargyl alcohol as corrosion inhibitor for nickel, copper, and copper/nickel (55/45) alloy. *Corrosion Science*, **2002**, 44(3), 467–479.

[29] Behpour, M., Ghoreishi, S., Soltani, N., Salavati-Niasari, M., Hamadanian, M., Gandomi, A. Electrochemical and theoretical investigation on the corrosion inhibition of mild steel by thiosalicylaldehyde derivatives in hydrochloric acid solution. *Corrosion Science*, **2008**, 50(8), 2172–2181.

[30] Saber, K., Hamouche, F., Hmada, A., Dkhireche, N., Hamzi, S., Galai, M. Degradation analysis of α-brass drinking water pipes in aggressive soil. *Journal of Applied Organometallic Chemistry*, **2024**, 4(3), 247–262.

[31] Hassani, Y., Bidi, H., Ebn Touhami, M., El Ouardighi, S., El Boulifi, H., Hamouche, F., Baymou, Y. Study of the corrosion behavior of lead-free α-brass ($CuZn_{21}Si_3P$) and (α+β)-brass ($CuZn_{36}Pb_2As$) in simulated drinking water and tap water. *Moroccan Journal of Chemistry*, **2024**, 12(2), 799–829.

[32] Bouchareb, F., Berredjem, M., Dehmchi, D.A., Kadri, R., Kadri, M., Ferkous, H., Mansouri, A., Bouyegh, S., Ahmed, S.A., Hadda, T.B. Synthesis, characterization, DFT/M06 studies, NBO, QTAIM and RDG analyses of new copper(II) complexes with bis-phosphonamide obtained under microwave irradiation. *Journal of Molecular Structure*, **2023**, 1294, 136503.

[33] Hamouche, F., Ebn Touhami, M., Hassani, Y.,Baymou, Y. Effect of cyclic temperature on the corrosion behavior of (α+β)-brass (CuZn36Pb2As) and α-brass (CuZn21Si3P) in tap water. *Journal of Applied Organometallic Chemistry*, **2024**, 4(1), 30–50.

[34] Hamouche, F., Ebn Touhami, M., Ech-Chebab, A., Larioui, A., Baymou, Y. Influence of cyclic temperature on the corrosion behavior of copper-zinc alloys in drinking water. *International Journal of Corrosion and Scale Inhibition*, **2023**, 12(4), 1883–1905.

[35] Hassan, H.M. Prevention of Corrosion in the Stainless Steel Metallic Using the Extract of Some Aquatic Plants. *Chemical Methodologies*, **2024**; 8(6): 462–477.

[36] Al-Sieadi, W.N., Al-Jeilawi, O.H., Khudhair, N.A., Shamaya, A.N., Abdulrahman, N.A. Synthesis and characterization of heterocyclic derivatives to evaluate their efficiency as corrosion inhibitors for carbon steel in saline medium. *Advanced Journal of Chemistry, Section A*, **2025**, 8, 209–219.

[37] Safi, M.N., Ahamed, L.S. Synthesis and experimental study of new coumarin derivatives as a corrosion inhibitor for carbon steel surface in 1 M HCl. *Advanced Journal of Chemistry, Sectrion A*, **2025**, 8(2), 256–277.

[38] Kumar, S., Kalia, V., Goyal, M., Jhaa, G., Kumar, S., Vashisht, H., Dahiya, H., Quraishi, M., Verma, C. Newly synthesized oxadiazole derivatives as corrosion inhibitors for mild steel in acidic medium: Experimental and theoretical approaches. *Journal of Molecular Liquids*, **2022**, 357, 119077.

[39] Chen, M.-F., Chen, Y., Lim, Z.J., Wong, M.W. Adsorption of imidazolium-based ionic liquids on the Fe (100) surface for corrosion inhibition: Physisorption or chemisorption?. *Journal of Molecular Liquids*, **2022**, 367, 120489.

[40] Hamad, O.A., Kareem, R.O., Azeez, Y.H., Kebiroğlu, M.H., Omer, R.A., Zebari, O.I.H. Quantum computing analysis of naphthalene compound: electronic structure, optical, and thermochemical approaches using DFT and HF. *Journal of Applied Organometallic Chemistry*, **2024**, 4(2), 100–118.

[41] Khadiri, M.-e., Benyaïch, A., Outzourhit, A., Ameziane, E.L. The corrosion behaviour of Ti-Cu (2%) in phosphoric acid. *Annales de Chimie Science des Matériaux*, **2000**, 25(6), 447–455.

[42] Alqudsi, A.M., Saleh, K.A. Electrochemical polymerization of eugenol and corrosion protection studies of stainless steel 304L alloy. *Journal of Medicinal and Chemical Sciences*, **2023**, 6(8), 1818–1829.

[43] Quartarone, G., Bonaldo, L., Tortato, C. Inhibitive action of indole-5-carboxylic acid towards corrosion of mild steel in deaerated 0.5 M sulfuric acid solutions. *Applied Surface Science*, **2006**, 252, 8251–8257.

[44] Soltani, N., Khayatkashani, M. Evaluating performance of malva sylvestris leaf extract for protection of mild steel against corrosion in acidic solution. *Asian Journal of Green Chemistry*, **2021**, 5, 39–57.

[45] Errahmany, N., Rouifi, Z., Kharbouch, O., Tazouti, A., Chahboune, M., Rbaa, M., Larhzil, H., Touir, R. Molecular structure of synthetized hydrazinylidene based quinoxaline derivatives effect on mild steel corrosion inhibition in 1.0 HCl electrolyte: Synthesis, electrochemical and computational studies. *Journal of Molecular Structure*, 2024, 1308, 138–146.

[46] Errahmany, N., Hamouche, F., Nounah, M., Saber, I., Yaqouti, S., Nounah, A., Tazouti, A., Rbaa, M., Fakhreddine, R., Touir, R. Theoretical and experimental studies of new synthetic quinoxaline derivatives as corrosion inhibitors for mild steel in a 1.0 M HCl environment. *Moroccan Journal of Chemistry*, **2024**, 12, 1707–1730.

[47] Wright, D., Liu, C.L., Stanley, D., Chen, H.C., Fang, J.H. Xrays: A fuzzy expert system for qualitative XRD analysis. *Computers & Geosciences*, **1993**, 19, 1429–1443

[48] Fujimura, A., Shoji, S., Kitagawa, Y., Hasegawa, Y., Doi, T., Fushimi, K. Development of a quasi-on-time ICP-OES for analyzing electrode reaction products. *Electrochimica Acta*, **2022**, 433, 141246.

[49] El Faydy, M., Touir, R., Ebn Touhami, M., Zarrouk, A., Jama, C., Lakhrissi, B., Olasunkanmi, L.O., Ebenso, E.E., Bentiss, F. Corrosion inhibition performance of newly synthesized 5-alkoxymethyl-8-hydroxyquinoline derivatives for carbon steel in 1 M HCl solution: experimental, DFT and Monte Carlo simulation studies. *Physical Chemistry Chemical Physics*, **2018**, 20(30), 20167–20187.

HOW TO CITE THIS ARTICLE

H. Malki, O. Kharbouch, F. Hamouche, N. Dkhireche, K. El Mabrouk, F. Elhajri, Z. Benzekri, S. Boukhris. Exploring Quinazolinone Compound as Corrosion Inhibitor for Mild Steel in Acidic Media: Electrochemical and Theoretical Studies. *Adv. J. Chem. A*, 2026, 9(6), 1155-1178.

DOI: 10.48309/AJCA.2026.546165.1994
URL: https://www.ajchem-a.com/article_239504.html